Oxygen torus in the deep inner magnetosphere and its contribution to recurrent process of O[+]-rich ring current formation

Nosé, M.; Takahashi, K.; Anderson, R. R.; Singer, H. J.

JOURNAL OF GEOPHYSICAL RESEARCH, VOL. 116, A10224, doi:10.1029/2011JA016651, 2011

Oxygen torus in the deep inner magnetosphere and its contribution to recurrent process of O^+-rich ring current formation

Nosé, M.,[1] K. Takahashi,[2] R. R. Anderson,[3] and H. J. Singer[4]

Abstract.

Using the magnetic fiel and plasma wave data obtained by the Combined Release and Radiation Effects Satellite (CRRES), we search for enhancements of O^+ ion density in the deep inner magnetosphere known as "the oxygen torus". We examine 4 events on the dayside in which toroidal standing Alfvén waves appear clearly. From the frequency of the toroidal waves, the magnetospheric local mass density (ρ_L) is estimated by solving the MHD wave equation for realistic models of the magnetic fiel and the fiel line mass distribution. We also estimate the local electron number density (n_{eL}) from the plasma wave spectrograms by identifying narrow-band emission at the upper-hybrid resonance frequency. Assuming the quasi-neutral condition of plasma, we infer the local average ion mass (M_L) by ρ_L/n_{eL}. It is found that M_L is approximately 3 amu in the plasma trough, while it shows an enhancement of >7 amu at L∼4.5-6.5 that is close to the plasmapause at L∼3.5-6.0. This indicates an existence of the oxygen torus in the vicinity of the plasmapause. The oxygen torus is found preferentially during the storm recovery phase. We interpret that these features of the oxygen torus (i.e., close relations with the plasmapause and the storm recovery phase) reflec its generation mechanism; that is, the ionospheric temperature is enhanced by heat conduction from high altitudes in the limited L range where the plasmasphere, because of its inflatio during the recovery phase, encounters the ring current, and then the ionosphere has a larger scale height and supplies O^+ ions to the inner magnetosphere, resulting in the oxygen torus. We also discuss the contribution of the oxygen torus to the formation of the O^+-rich ring current. It is proposed that the O^+-rich ring current is formed in a recurrent process, in which the oxygen torus, the plasmasphere, and the ring current interact with each other.

1. Introduction

The plasmaspheric ion composition is an important issue in terrestrial plasma environment and has been studied by using the retarding ion mass spectrometer (RIMS) instrument on board the Dynamic Explorer (DE) -1 satellite, which was capable of measuring the pitch angle and energy spectral characteristics of ions in a mass range of 1-32 amu and in an energy range of 0-45 eV [*Chappell*, 1982]. After the DE-1 satellite was launched into a polar orbit, with an apogee of 4.6 R_E geocentric altitude in August 1981 [*Hoffman*, 1988], the RIMS instrument collected thermal plasma data in the plasmasphere and the inner magnetosphere from 1981 to 1989. *Chappell* [1982] firs reported a difference in the radial flu distribution between light ions (H^+ and He^+) and heavy ions (O^+ and O^{2+}); that is, these ions are all present in the plasmasphere, but O^+ and O^{2+} are located at higher L-shells than H^+ and He^+. O^+ and O^{2+} flu es are even enhanced outside of the plasmapause that is determined by the H^+ and He^+ radial profile Chappell concluded the existence of a torus of O^+ and O^{2+} ions in the outer plasmasphere. This "oxygen torus" has been identifie in subsequent studies using the DE-1/RIMS data [*Horwitz et al.*, 1984, 1986; *Roberts et al.*, 1987; *Comfort et al.*, 1988]. *Horwitz et al.* [1984, 1986] showed that the O^+ and O^{2+} densities become comparable to or exceeds the H^+ density at L=3-4. A statistical analysis of the oxygen torus (identifie by O^+ and O^{2+} ions) was made by *Roberts et al.* [1987], who found that (1) the oxygen torus is observed just inside the plasmasphere at all local time with higher occurrence frequency in the late evening and morning sectors, (2) it is identifie on ∼50% of orbits, (3) its occurrence frequency does not depend on the Kp index and is still fairly high even in the low Kp case (Kp=0-2+), and (4) a density peak of the oxygen torus generally shifts toward lower L shell with increasing geomagnetic activity. *Comfort et al.* [1988] also performed a statistical study and showed an enhancement of O^+ and O^{2+} ions in the outer plasmasphere (L=3-5). These studies substantiate an enhanced population of thermal O^+ and O^{2+} ions at L=3-5 (i.e., the oxygen torus) in both quiet and disturbed times. Even coexistence of N^+ ions within the oxygen torus is noted by *Horwitz et al.* [1986] and *Roberts et al.* [1987].

A recent study by *Nosé et al.* [2010] casts a new light on the oxygen torus in terms of the possibility that it plays an important role in generation of an O^+-rich ring current. They found that magnetic fiel dipolarization in the deep inner magnetosphere (L=3.5-5.0) is not unusual. Magnetic fiel dipolarization was accompanied by magnetic fiel fluctuation having a characteristic timescale of 3-5 s, which is comparable to the local gyroperiod of O^+ ions. After dipolarization, the energetic neutral atom (ENA) flu of oxygen in the nightside ring current region was suddenly enhanced by a factor of 2-5 and stayed at an enhanced level for more than one hour, while a clear enhancement was scarcely seen in the hydrogen ENA flux On the basis of these observational results, *Nosé et al.* [2010] proposed a new scenario for the generation of an O^+-rich ring current, in which the thermal O^+ ions preexisting in the oxygen torus are locally and nonadiabatically accelerated by fluctuation associated with dipolarization in the deep inner magnetosphere (L=3.5-5.0). Therefore a more detailed investigation of the oxygen torus may give a clue to understand the long-time, unresolved problem

[1]Data Analysis Center for Geomagnetism and Space Magnetism, Graduate School of Science, Kyoto University, Kyoto, Japan.
[2]Applied Physics Laboratory, Johns Hopkins University, Laurel, Maryland, USA.
[3]Department of Physics and Astronomy, University of Iowa, Iowa City, Iowa, USA.
[4]NOAA/National Weather Service, National Centers for Environmental Prediction, Space Weather Prediction Center, Boulder, Colorado, USA.

0148-0227/11/2011JA016651$9.00

regarding the dynamics of ions of ionospheric origin in the ring current region [e.g., *Kamide et al.*, 1997; *Daglis and Kozyra*, 2002; *Daglis*, 2006].

Unfortunately, since the termination of the DE-1/RIMS operation ∼20 years ago, there have been no direct measurements of the oxygen torus, because of the difficult in measuring thermal ion flu with mass and charge state information. The present study intends to detect the oxygen torus with an indirect method using the magnetic fiel data and the plasma wave data obtained by the Combined Release and Radiation Effects Satellite (CRRES). We estimate the magnetospheric local mass density (ρ_L) from the frequency of the toroidal standing Alfvén waves. The local electron number density (n_{eL}) is derived from the plasma wave spectra. Combining these two quantities makes it possible to infer the local average ion mass ($M_L \sim \rho_L / n_{eL}$). Such indirect method of analysis has been adopted by previous studies. *Denton et al.* [2004] and *Takahashi et al.* [2004, 2008] analyzed the same data set from the CRRES satellite. They inferred a concentration of heavy ions at the magnetic equator and an enhancement of the average ion mass between the plasmapause and the plasma plume. From measurements of the standing wave frequency using ground magnetic fiel data, the equatorial plasma mass density has been also indirectly estimated by *Fraser et al.* [2005], *Grew et al.* [2007], *Maeda et al.* [2009], and *Obana et al.* [2010]. In these studies, to estimate the average ion mass, the electron number density was determined from the plasma waves in space [*Fraser et al.*, 2005; *Maeda et al.*, 2009] or the VLF whistler waves on the ground [*Grew et al.*, 2007; *Obana et al.*, 2010].

The organization of this paper is as follows. In section 2, we describe the instrumentation and data set. In section 3, magnetic fiel data from the CRRES satellite are presented. We perform a frequency analysis of 4 toroidal standing Alfvén wave events. In section 4, a methodology to estimate plasma mass density from the toroidal wave frequency is explained and results of the estimates for the 4 events are shown. In section 5, we obtain the electron number density from the plasma wave spectrograms. Combining the results of the plasma mass density and the electron number density, we estimate the average plasma mass and fin the oxygen torus near the plasmapause. In section 6, we will compare the present results with those by DE-1/RIMS in terms of the radial and MLT distributions, the ion composition, and the dependence on geomagnetic condition. A generation mechanism for the oxygen torus and its role in the O^+-rich ring current formation will be discussed. Section 7 provides conclusions of this paper.

2. Instrumentation and Data Set

2.1. CRRES Satellite

The CRRES satellite was launched on 25 July 1990 into an elliptical orbit having initially a perigee of 1.05 R_E, an apogee of 6.27 R_E, an inclination of 18°, and an orbital period of 9.9 h. The satellite spun at a rate of 2.0 rpm and its spin axis was lying in the ecliptic plane with pointing 5°-15° ahead of the Sun's apparent motion. The apogee was firs placed around 0800 magnetic local time (MLT) and rotated toward the earlier local time with an apsidal precession of ∼0.7°/day. The operation ended in October 1991. An overview of the CRRES mission is described by the work by *Johnson and Kierein* [1992].

2.2. Magnetic Field

The CRRES satellite carried a triaxial flux ate magnetometer, which was mounted at the end of a 6.1-m boom to reduce any satellite-generated magnetic fiel [*Singer et al.*, 1992]. The magnetic fiel was measured with a sampling rate of ∼16 Hz and was operated with two observation modes; the dynamic range and resolution of each mode are ±45,000 nT and 22 nT (low-gain mode), and ±850 nT and 0.43 nT (high-gain mode). The high gain mode was switched on beyond the radial distance of about 3.5 R_E.

In this study we use 2-s average magnetic fiel data that are made from the high gain mode data. We subtract the tenth-generation International Geomagnetic Reference Field (IGRF) model from the 2-s average data, and create data file that contain the magnetic fiel deviation from the model. Data in these file are ΔB_V, ΔB_D, and ΔB_H in Vehicle-Dipole-Horizon (VDH) coordinates, where H is antiparallel to the dipole axis, V points radially outward and is parallel to the magnetic equator, and D is eastward and completes a right-handed orthogonal system.

2.3. Electron Number Density

The local electron number density (n_{eL}) is estimated from plasma wave data that are obtained by the plasma wave experiment onboard the CRRES satellite. The plasma wave experiment provides measurements of electric field from a 14-channel spectrum analyzer covering the frequency range of 5.6 Hz to 10 kHz and a 128-step sweep frequency receiver covering the frequency range of 10 kHz to 400 kHz [*Anderson et al.*, 1992]. The sweep frequency receiver has four frequency bands with 32 steps per band: Band 1 (100 Hz-800 Hz), Band 2 (800 Hz-6.4 kHz), Band 3 (6.4 kHz-50 kHz), and Band 4 (50-400 kHz). These frequency bands produce one spectrum at every 32 s, 16 s, 8 s, and 8 s, respectively.

Scanning plasma wave spectrograms for the electric field we identifie narrow-band emission at the upper hybrid resonance frequency (f_{UHR}), which is given by

$$f_{\mathrm{UHR}} = \sqrt{f_{pe}^2 + f_{ce}^2} = \frac{1}{2\pi}\sqrt{\frac{n_{eL}e^2}{\varepsilon_0 m_e} + \left(\frac{eB}{m_e}\right)^2}, \qquad (1)$$

where f_{pe} is the plasma frequency, f_{ce} is the electron cyclotron frequency, e is the electron charge, ε_0 is the vacuum permittivity, m_e is the electron mass, and B is the magnetic fiel intensity. Once f_{UHR} is determined from the spectrogram, n_{eL} can be calculated from equation (1) with a value of B measured by the flux ate magnetometer [*LeDocq et al.*, 1994]. Since the emission at f_{UHR} usually appeared in Band 3 and 4, this procedure was done every 8 s.

3. Observations

We examine 4 events of toroidal ULF waves, all of which are found in 3.5-hour CRRES orbit segments. These 4 events are selected as typical examples of successful detection of the oxygen torus by the present indirect method. First, we will show 2 events appeared near local noon. Then, a duskside event and a dawnside event will be displayed. MLT is not considered in selection of events, but no events are found on the nightside. We also do not consider geomagnetic condition in the event selection; nevertheless, these 4 events are found during the storm recovery phase, as shown later. Discussion about the MLT preference and the geomagnetic storm dependence will be given in section 6.1.

Figure 1 shows the orbit segments of these events in the XY plane in solar magnetospheric (SM) coordinates. In event 1 (27 August 1991, Orbit 961) and event 2 (11 September 1991, Orbit 996), CRRES moved from local noon to the afternoon sector. In event 3 (24 July 1991, Orbit 881), CRRES moved from the afternoon sector towards the dusk sector. Event 4 (29 August 1990, Orbit 84) was found in the dawn sector.

3.1. Event 1: 27 August 1991 (Orbit 961)

The top panel of Figure 2 shows the magnetic fiel variations in the D component (ΔB_D) for 1130-1500 UT on 27 August 1991 (Event 1). ΔB_D is low-pass filtere with a cutoff period of 30 s. In this event, the CRRES satellite was on Orbit 961 and traversed from L=4.0 to L=6.6 in the early afternoon sector (MLT=11.9-15.1 h). In the inner magnetosphere around L=4.0-5.0 (1140-1210 UT), a toroidal wave is clearly identifie with a period (T) of ∼4 min. When the satellite moves toward outer magnetosphere, there are still toroidal waves having T∼4 min, but shorter-period waves become apparent.

In order to examine frequency changes of the toroidal waves, we create a dynamic power spectrum as shown in the bottom panel of Figure 2. The power spectra are calculated by applying fast Fourier transformation to time series of ΔB_D in a moving 1024-s (i.e., 512 data points) time window that is shifted by 256 s (i.e., 128 data points) in successive steps. From this panel, we can fin that toroidal waves with the frequency of 4-5 mHz are prevailing during the 3.5-h interval. The shorter-period waves stated above are recognized by power enhancements lying from ~23 mHz around 1300 UT to ~18 mHz around 1430 UT. We interpret that these two kinds of toroidal waves are the fundamental and 3rd harmonics of the standing Alfvén waves, because the CRRES satellite was located off the equatorial plane (geomagnetic latitude (GMLAT) of -10° to -16°), where the odd-mode standing waves have a larger amplitude in magnetic fiel oscillations than near the equatorial plane [e.g., *Takahashi and Anderson*, 1992]. Since the fundamental mode oscillation has larger power and appears rather continuously, we use its peak frequency to infer plasma mass density. The peak frequency of the fundamental mode (f_1) is firs selected with the following criteria: (1) $P(f_1-2\Delta f)<P(f_1-\Delta f)<P(f_1)$ and $P(f_1)>P(f_1+\Delta f)>P(f_1+2\Delta f)$, and (2) $P(f_1)\geq 10^{0.5}$ nT^2/Hz, where $P(f)$ is the wave power at frequency f, and Δf is an increment of frequency, being 0.98 mHz (=1/1024 Hz) in this case. This is followed by a visual comparison of the f_1 values and the dynamic power spectrum to reject values that do not match the fundamental harmonic line seen in the dynamic power spectrum. The f_1 samples that passed these steps are plotted with open circles over the dynamic power spectrum. In a later section (section 4), the plasma mass density will be estimated from these selected f_1 values.

3.2. Event 2: 11 September 1991 (Orbit 996)

Figure 3 displays ΔB_D and its dynamic power spectrum of event 2 in the same format as Figure 2. This event was found during 1200-1530 UT on 11 September 1991. The CRRES satellite was on Orbit 996 and moved from L=3.3 to L=6.4 in local noon and the early afternoon (MLT=10.9-14.4 h). The top panel of Figure 3 shows pronounced wave activity for most of the interval. The wave period is about 2 min from 1200 UT to 1230 UT, while it becomes longer, ~4 min, around 1240-1255 UT. After 1300 UT, shorter period components are superimposed on the long period wave. These features can be seen more clearly in the dynamic power spectrum. There are two frequency bands which decreases from ~8 mHz to ~3 mHz and from ~25 mHz to ~15 mHz as the satellite moves towards the outer magnetosphere. Since the satellite was off the equator, these bands are considered to be the fundamental and the 3rd harmonics of the standing Alfvén waves. In the same way as done in event 1, we determine f_1 that are indicated over the dynamic power spectrum with open circles. We note that the wave observed around 1240-1255 UT has lower frequency than those observed in adjacent time intervals (i.e., 1225-1240 UT and 1255-1310 UT).

3.3. Event 3: 24 July 1991 (Orbit 881)

Figure 4 shows ΔB_D and its dynamic power spectrum of event 3. In this event, the CRRES satellite was on Orbit 881 and moved from L=5.1 to L=7.7 on the late afternoon sector (MLT=14.6-17.0 h) during 0330-0700 UT on 24 July 1991. ΔB_D in the top panel indicates that a rather monotonic wave with T~5 min appeared for the whole time interval, although amplitude becomes larger after 0500 UT. The dynamic power spectrum in the bottom panel confirm the monotonic toroidal waves around 3-4 mHz. It should be noted that in the innermost range of L=5.1-6.5 (i.e., during 0330-0430 UT), the wave frequency becomes lower when the satellite is located closer to the Earth.

3.4. Event 4: 29 August 1990 (Orbit 84)

Figure 5 shows ΔB_D and its dynamic power spectrum of event 4 for 0930-1300 UT on 29 August 1990, in which the CRRES satellite was on Orbit 84 and passed through L=3.9-7.5 on the dawn side (MLT=3.6-6.4 h). We can see that toroidal waves of T~4 min appeared in ΔB_D from 1000 UT to 1300 UT. The amplitude of the waves suddenly enhanced around 1123 UT. There were no high-time resolution solar wind data on this day, but we believe that this enhancement was caused by an increase of the solar wind dynamic pressure, because the SYM-H index increased by ~20 nT at the same time (not shown here). From the dynamic power spectrum in the bottom panel we fin the toroidal waves were rather monotonic around 4 mHz. However, we also note that in the L range of 4.9-6.3 (i.e., 1005-1100 UT), the frequency is lower at lower L.

4. Estimation of Plasma Mass Density

4.1. Methodology

It is possible to estimate the magnetospheric local mass density (ρ_L) from the frequency of the fundamental mode of the toroidal standing Alfvén waves (f_1). With the time of fligh approximation, f_1 is given by

$$f_1 = \left\{ 2\int_{s1}^{s2} \frac{ds}{V_A(s)} \right\}^{-1} = \left\{ 2\int_{s1}^{s2} ds \frac{\sqrt{\mu_0 \rho(s)}}{B(s)} \right\}^{-1}, \quad (2)$$

where a variable s represents the distance from the ground in the northern hemisphere along the magnetic fiel line, V_A is the Alfvén wave velocity, μ_0 is the vacuum permeability, ρ is the mass density. The integral is computed from the northern ionosphere (s_1) to the southern ionosphere (s_2). The distribution of the mass density along the magnetic fiel line, $\rho(s)$, can be modeled by a power law form [e.g., *Takahashi and Anderson*, 1992; *Denton et al.*, 2002]:

$$\rho(s) = \rho_{\rm eq} \left(\frac{LR_E}{r} \right)^{\alpha}, \quad (3)$$

where $\rho_{\rm eq}$ is the equatorial mass density, r is the geocentric distance to the fiel line, and α is the power law index. Note that r can be expressed as a function of s, that is, r=$r(s)$, because equation (3) is applied to a fiel line specifie by r=LR_E at the equator. With substitution of equation (3) into equation (2), f_1 is found to be inversely proportional to $\sqrt{\rho_{\rm eq}}$, that is, $f_1 \propto 1/\sqrt{\rho_{\rm eq}}$. Choosing an appropriate geomagnetic fiel model, we can numerically integrate equation (2) and fin $\rho_{\rm eq}$ that gives the observed f_1. Then this $\rho_{\rm eq}$ is converted to ρ_L by using equation (3).

However, when the wave length becomes comparable to the length of the magnetic fiel line, the above approximation is invalid. In this case, we need to solve the MHD wave equations. *Singer et al.* [1981] wrote the decoupled transverse MHD wave equation including a general magnetic fiel geometry in the following form:

$$\frac{\partial^2}{\partial s^2}\left(\frac{\xi(s)}{h(s)}\right) + \frac{\partial}{\partial s}\ln\left\{h(s)^2 B(s)\right\}\frac{\partial}{\partial s}\left(\frac{\xi(s)}{h(s)}\right) + \left(2\pi f_1 \frac{\sqrt{\mu_0\rho(s)}}{B(s)}\right)^2 \left(\frac{\xi(s)}{h(s)}\right) = 0, \quad (4)$$

where ξ is the displacement of the magnetic fiel line, and h is a factor describing separation between two adjacent fil lines (it becomes smaller as being far from the equator). The equation looks complicated, but a background concept is similar to that in equation (2); for instance, the inverse proportion between f_1 and $\sqrt{\rho_{\rm eq}}$ is still held in equation (4). The task is to numerically solve equation (4) with insertion of equation (3) and to fin $\rho_{\rm eq}$ that satisfie $\xi(s_1)$=$\xi(s_2)$=0 and $\xi(s_1<s<s_2)\neq 0$ for the observed f_1. Once $\rho_{\rm eq}$ is obtained, we can calculate ρ_L from equation (3).

4.2. ρ_L of Events 1-4

In calculating ρ_L from f_1 for events 1-4, we take s_1 and s_2 to be the ionospheric height of 200 km for both hemispheres. For

the magnetic field we adopt the Tsyganenko 1989c (T89c) model [*Tsyganenko*, 1989]. The T89c model requires the Kp index as an input parameter and we use the Kp value at the beginning of the 3.5-h interval for each event. The power law index in equation (3) is taken to be α=0.5, because recent studies reported α=0.2-0.9 at L=3.5-5.5 [*Denton et al.*, 2002] and $\alpha\sim$0.5 at L=4-6 [*Takahashi et al.*, 2004].

Four panels in the top row of Figure 6, from left to right, display the f_1 values of events 1-4 that are determined in Figures 2-5. Following the method described above, we estimate ρ_L from f_1 and the results are shown in the second row of Figure 6. Error bars indicate the range of ρ_L when the f_1 values have a determination error of Δf; that is, f_1 ranges from $f_1+\frac{1}{2}\Delta f$ to $f_1-\frac{1}{2}\Delta f$. ρ_L was decreasing generally as the CRRES satellite moves far from the Earth. We also notice that small deviations of ρ_L from the general decreasing trend are anticorrelated with those of f_1, as expected from the inverse proportion between them found in equation (4).

5. Estimation of Average Plasma Mass

5.1. Methodology

We obtain the local electron number density (n_{eL}) from the plasma wave spectrograms by identifying the narrow-band emission at f_{UHR}. From the quasi-neutrality of plasma, we assume that the local ion number density summed over the ith singly-charged ion species ($\sum_i n_{iL}$) is nearly equal to n_{eL} (i.e., $\sum_i n_{iL}\sim n_{eL}$). Letting m_i be the mass of the ith singly-charged ion species and M_L be the local average plasma mass, we can express ρ_L by

$$\rho_L = n_{eL}m_e + \sum_i n_{iL}m_i \sim \sum_i n_{iL}m_i = \sum_i n_{iL}\left(\frac{\sum_i n_{iL}m_i}{\sum_i n_{iL}}\right) \sim n_{eL}M_L. \quad (5)$$

Therefore we can infer M_L by ρ_L/n_{eL}.

5.2. M_L of Events 1-4

The third row of Figure 6 displays n_{eL} derived from the plasma wave spectrograms for events 1-4. At the beginning of plots, n_{eL} is larger than 10^3 cm^{-3}, indicating that the CRRES satellite was in the plasmasphere. Then n_{eL} shows a steeper decrease in a limited UT range than in other UT range; that is, around 1200 UT in event 1, during 1200-1230 UT in event 2, and around 0240 UT in event 3. This is due to a plasmapause crossing by the CRRES satellite. In event 4, n_{eL} shows disturbances between $\sim$3 cm^{-3} and $\sim$30 cm^{-3} for 1020-1050 UT, which are considered as a result of multiple crossings of the plasmapause by CRRES. After passing through the plasmapause, n_{eL} is in the order of 10 cm^{-3} or less, suggesting the plasma trough.

Following equation (5), we calculate M_L from the data shown in the panels in the second (ρ_L) and the third (n_{eL}) rows, and show the results in the bottom row. In all of the events, the plasma trough has $M_L\sim$2-5 amu, which is consistent with a statistical result of $M_L\sim$3 amu by *Takahashi et al.* [2006]. It is noticed that M_L is enhanced to 7-8 amu in events 1 and 2. These enhancements occur just around when CRRES traversed the plasmapause. Event 3 shows M_L enhancement of 15-18 amu at 0330-0350 UT. Although we have no information of M_L before 0330 UT, it may be possible that the enhancement is spread down to near the plasmapause. In event 4, M_L is enhanced to 15-17 amu at 1005-1025 UT and to 7 amu around 1110 UT. These M_L enhancements appear just inside and outside of the plasmapause. The large value of $M_L>$7 amu suggests that plasma contains heavy ions such as O^+ (m_{O^+}=16 amu) in addition to H^+ (m_{H^+}=1 amu) and He^+ (m_{He^+}=4 amu). For instance, the average mass of plasma with 50% H^+ and 50% O^+ is 8.5 amu. If we consider a contribution from He^+ with the He^+/H^+ density ratio of $\sim$0.2 [*Comfort et al.*, 1988; *Newberry et al.*, 1989], plasma with 45% H^+, 10% He^+, and 45% O^+ gives $M_L\sim$8 amu. (We found M_L being more than 16 amu in some data points of events 3 and 4, that is, the flanksid events, which is unreasonable from the viewpoint of magnetospheric plasma. It is supposed that the mass density distribution model of equation (3) and/or the magnetic fiel model may not describe the actual conditions properly for these data points. The reason for this supposition is because *Takahashi and Denton* [2007] reported a local peak of ρ at the geomagnetic equator in the late afternoon sector, which can not be expressed by equation (3), and the actual geomagnetic fiel on the flankside is stretched tailward and possibly deviated from the model field Even so, we presume these data points indicate that the plasma is heavily loaded by O^+ ions.) Therefore it is concluded that these 4 events showed enhancements of O^+ ion density near the plasmapause.

In order to examine locations of the plasmapause and the O^+ density enhancement in the inner magnetosphere, we redraw the n_{eL} and M_L data as a function of the L-value, as shown in Figure 7. The plasmapause is visually identifie as stated in the beginning of this section, and is located at L=4.6-5.0 (event 1), L=3.5-4.3 (event 2), L=3.4-3.6 (event 3), and L=5.4-6.1 (event 4). The O^+ density enhancement is located at $L\sim$5.0-5.2 (event 1), $L\sim$4.5-4.8 (event 2), $L\leq$5.6 (event 3), and $L\sim$5.0-6.5 (event 4). Existence of the O^+ density enhancement in the limited L range indicates the formation of an oxygen torus. Comparing the L-values between the plasmapause and the oxygen torus, we fin that the oxygen torus is placed just outside the plasmapause (events 1 and 2), extends outside the plasmapause (event 3), and coexists with the plasmapause (event 4).

6. Discussion

6.1. Comparison with DE-1/RIMS Results

The oxygen torus was firs reported by *Chappell* [1982], and then investigated in subsequent studies of *Horwitz et al.* [1984, 1986], *Roberts et al.* [1987], and *Comfort et al.* [1988]. All of these previous studies utilized the DE-1/RIMS data. We will compare our results about the oxygen torus obtained by the indirect method with those obtained by ion flu measurements of DE-1/RIMS.

6.1.1. Radial and MLT Distribution

Previous studies employing DE-1/RIMS data reported that the oxygen torus is found at L=3.7-5.0 [*Chappell*, 1982], at L=3.0-4.0 [*Horwitz et al.*, 1984, 1986], at $L\sim$3-5 with an average of just inside L=4 [*Roberts et al.*, 1987], and at $L\sim$4 [*Comfort et al.*, 1988]. *Chappell* [1982] and *Horwitz et al.* [1984] further reported that the oxygen torus is located in the vicinity of or outside the plasmapause that was identifie by H^+ density. In this study we found the oxygen torus at L=4.5-5.6, which is larger than the DE-1 results (L=3.0-5.0). However, this difference is not significan since the relative locations to the plasmapause are the same for both results (i.e., in the vicinity of the plasmapause). Therefore we believe that a radial distribution of the oxygen torus detected by the indirect method is consistent with those by the direct measurement of DE-1/RIMS.

According to *Roberts et al.* [1987], the O^+ density enhancements are observable in all local time zones. The occurrence frequency is 70% or higher in the late evening hours (2000-2400 UT) and in the early morning hours (0500-0900 MLT). In this study, the oxygen torus is found in local noon or on the early afternoon sector (events 1 and 2), on the late afternoon sector (event 3), and on the dawn side (event 4), which cover the dayside hemisphere. Unfortunately, no events are found in the nightside hemisphere. We suggest that this is not because no oxygen torus is formed, but because toroidal standing Alfvén waves are scarcely excited by low ionospheric conductivity as well as a large separation from the dayside energy sources [e.g., *Anderson et al.*, 1990; *Chi et al.*, 2005]. For the oxygen torus on the sunlit hemisphere, at least, we can conclude that the distribution is consistent with the DE-1/RIMS result.

6.1.2. Ion Composition

Horwitz et al. [1984] revealed that the O^+ density reaches $\sim$100 cm^{-3} and can become comparable to the H^+ density in the oxygen torus; that is, the O^+/H^+ density ratio (n_{O+}/n_{H+}) becomes $\sim$1.0. These features are also recognized in Figures 3b and 3c of *Horwitz et al.* [1986] and in Figures 3 and 5 of *Roberts et al.*

[1987]. From these observations we can calculate as M_L=8.5 amu for n_{O+}/n_{H+}=1.0. This value of M_L is in agreement with the present result of M_L>7 amu.

6.1.3. Dependence on Geomagnetic Condition

Roberts et al. [1987] found that an occurrence frequency of the oxygen torus does not depend on the Kp index and is still fairly high (40-70%) even in quiet period (Kp=0-2+). We note that the Kp index at the beginning of events 1-4 is 2○, 4+, 4−, and 2−, respectively, indicating rather moderate geomagnetic condition. This result seems to represent no clear dependence of occurrence probability on geomagnetic condition, being consistent with the results by *Roberts et al.* [1987].

In order to examine storm phases during the 4 events, we plotted the Dst index in Figure 8. A closed circle at the bottom of each panel indicates the 3.5-h interval of each event. We see that events 1, 3, and 4 are found during the late recovery phase or at the end of magnetic storms. Although event 2 occurred during the main phase of a small magnetic storm having a Dst peak value of -41 nT, it is included in the recovery phase of a larger magnetic storm during the interval 9-13 September 1991. This investigation leads us to surmise that the oxygen torus favorably occurs during the storm recovery phase. However, it should be kept in mind that the investigation is based on case studies of only 4 events and does not provide very strong support for the notion. The storm phase dependence will be reexamined in a future statistical study.

Roberts et al. [1987] found that the location of the O^+ density enhancement peak is dependent to the Dst index and is define by

$$L_{\text{peak}} < \frac{1}{15}\text{Dst} + 7. \quad (6)$$

In the present 4 events, the Dst values at the beginning of the 3.5-hour interval are -17 nT, -41 nT, -18 nT, and -4 nT, respectively. Insertion of these values into the equation (6) leads to estimation of the O^+ density peaks at L_{peak}<5.9, L_{peak}<4.3, L_{peak}<5.8, and L_{peak}<6.7. From Figure 7, we identify the O^+ density peaks at L=5.2-5.6, L=4.7, L<5.4, and L=5.4, for events 1-4. All but event 2 agree with the estimation by equation (6). For event 2, the discrepancy of the peak L values is as small as ∼0.4. Therefore we consider that our observational results are generally consistent with those by *Roberts et al.* [1987] in terms of the Dst dependence of the L shell of the O^+ density enhancement peak.

6.2. Generation Mechanism of Oxygen Torus

The key features of the oxygen torus in considering its generation mechanism are that (1) it is found near the plasmapause; (2) it is observable in all local time zones with higher occurrence frequencies in the late evening and early morning hours; and (3) it may be likely to occur during the storm recovery phase. (The third feature is based on the discussion in section 6.1.3; thus it is still a working assumption.) It is well known that the plasmasphere expands during the storm recovery phase [e.g., *Taylor et al.*, 1968; *Chappell et al.*, 1970]. This expansion is predicted to occur in all local times by plasmapause models [*Carpenter and Anderson*, 1992; *Gallagher et al.*, 2000; *Moldwin et al.*, 2002]. Therefore generation of the oxygen torus may be related to the expansion of the plasmasphere.

During the storm main phase, the westward ring current fl ws predominantly from the nightside to the duskside and is axially asymmetric, but it gradually becomes more symmetric during the storm recovery phase [e.g., *Nakabe et al.*, 1997; *Terada et al.*, 1998; *Mitchell et al.*, 2001; *C:son Brandt et al.*, 2002]. A main portion of the westward current is found at L∼4-7 [e.g., *McEntire et al.*, 1985; *Lui et al.*, 1987; *Le et al.*, 2004]. According to satellite observations (OGO 5, ISEE 1, and CRRES), the plasmapause shifts to lower L shells (L∼3-4) during disturbed periods, while it moves to L=5-6 during quiet periods [*Chappell et al.*, 1970; *Carpenter and Anderson*, 1992; *Moldwin et al.*, 2002]. Thus the plasmapause encounters the symmetric ring current around L=4-6 after the main phase of the magnetic storms. Interaction between energetic ring current ions and cold plasma was discussed by *Cole* [1965] and *Cornwall et al.* [1971]. *Cole* [1965] proposed Coulomb collision as an energy transfer process from ring current protons to thermal plasmaspheric electrons. According to *Cornwall et al.* [1971], when the cold plasma density is on the order of 100 cm^{-3} or higher, ring current protons with 10-50 keV energies become unstable and generate intense ion cyclotron wave turbulence. Then the ion cyclotron wave is absorbed by plasmaspheric thermal electrons through the Landau resonance interaction. A review on the energy transfer from ring current ions to thermal plasma (including both electrons and ions) is given by *Comfort* [1996]. Whichever of these processes is dominant, plasmaspheric thermal electrons are heated. The resultant heat is conducted down to the underlying ionosphere and raises the temperatures of ionospheric ions and electrons. This results in increases of the scale height of ionospheric plasma. Since the scale height of O^+ ions is normally much smaller than H^+ ions, even a small rise in scale height affects density changes at the topside ionosphere more strongly for O^+ ions than for H^+ ions [*Yau et al.*, 1985; *Nosé et al.*, 2009]. This causes a large number of O^+ ions to diffuse into the high altitude and form the oxygen torus in the limited L-shell where the ring current and the plasmasphere coexist.

The above mechanism has been proposed by *Horwitz et al.* [1986], who found that the plasmaspheric enhancement of O^+ ions is often closely aligned with distinct and isolated electron temperature enhancement above the ionospheric altitude. *Horwitz et al.* [1990] also reported the similar result, that is, the latitudinal correspondence between the O^+ density enhancement in the inner magnetosphere and the ionospheric electron temperature enhancement. *Roberts et al.* [1987] discussed that observed characteristics of the oxygen torus support this mechanism. We think that the aforementioned three key features of the oxygen torus are consistent with what is expected from this mechanism.

6.3. Oxygen Torus as Possible Source of O^+-rich Ring Current

6.3.1. Outline of Previous Studies on O^+-rich Ring Current

It has been reported that the ion composition of the ring current changes drastically during magnetic storms. Using the energetic (1-300 keV) ion flu data obtained by the AMPTE/CCE satellite, *Gloeckler et al.* [1985], *Krimigis et al.* [1985], *Hamilton et al.* [1988], and *Feldstein et al.* [2000] revealed that the O^+/H^+ energy density ratio changes from 0.01-0.03 (quiet times) to 0.3-0.6 (storm times) in the outer ring current region of L=5-7. *Greenspan and Hamilton* [2002] made a statistical analysis of the AMPTE/CCE data and found the O^+/H^+ energy density ratio at L=2-7 to be ∼0.3 during magnetic storms. From analysis of the energetic (50-430 keV) ion flu measured by the CRRES satellite, *Roeder et al.* [1996], *Daglis* [1997], and *Daglis et al.* [2000] found that the O^+/H^+ energy density ratio changes from 0.1-0.3 (quiet times) to 0.3-3.0 (storm times) at L=3-7. *Nosé et al.* [2005] estimated that the O^+/H^+ energy density ratio in the ring current was as large as 10-20 for the October 2003 superstorm.

Some scenarios have been proposed to explain this strong enhancement of O^+ energy density in the ring current. The scenarios include (1) direct transport of O^+ ions from the ionosphere to the ring current [e.g., *Daglis et al.*, 1994; *Gazey et al.*, 1996]; (2) transport of O^+ ions, following the path from the ionosphere, to the magnetic lobe, to the near-Earth plasma sheet, followed by adiabatic transport into the ring current and betatron acceleration [e.g., *Lui et al.*, 1986; *Lui*, 1993]; and (3) transport of O^+ ions, following the path from the ionosphere, to the magnetic lobe, to the near-Earth plasma sheet, followed by nonadiabatic transport and acceleration by an inductive electric fiel resulting from the magnetic fiel dipolarization [e.g., *Delcourt et al.*, 1990; *Sánchez et al.*, 1993; *Mitchell et al.*, 2003; *Ohtani et al.*, 2005]. However, it is not yet elucidated as to what scenario is responsible for the formation of O^+-rich ring current.

Recently, *Nosé et al.* [2010] studied magnetic fiel reconfigu ration and associated ion acceleration in the deep inner magnetosphere, using the MDS-1 and IMAGE satellites. It was found that dipolarization occurs even in the range L=3.5-5.0 during the storm main phases and is accompanied by magnetic fiel fluctuation with

a characteristic time scale comparable to the local O^+ gyroperiod. After dipolarization, the oxygen ENA flu in the nightside ring current region greatly increased by a factor of 2-5, whereas the hydrogen ENA flu in the same region showed insignifican enhancement. The oxygen ENA flu was maintained at an enhanced level for more than one hour. From these observational results, *Nosé et al.* [2010] proposed a new scenario for the generation of the O^+-rich ring current, in which the preexisting thermal O^+ ions in the oxygen torus experience local and nonadiabatic acceleration by magnetic fiel fluctuation that accompany dipolarization in the deep inner magnetosphere (L=3.5-5.0) and contribute to the O^+-rich ring current formation.

6.3.2. Recurrent Process of O^+-rich Ring Current Formation

On the basis of the new scenario by *Nosé et al.* [2010] and the present results, we propose a recurrent process of the O^+-rich ring current formation, as shown schematically in Figure 9. At a starting point, the oxygen torus is placed close to the plasmapause during the late recovery phase, as we found in events 1-4 (Figure 9a). The torus will remain there in quiet times after a storm ends. When the interplanetary magnetic fiel turns southward, often with increased solar wind speed, a magnetic storm starts. During the storm main phase, the ring current begins to develop on the nightside and the outer layer of the plasmasphere is eroded, resulting in a shrinking of the plasmasphere (Figure 9b). The eroded plasma drifts sunward and is drained away with formation of the plasmaspheric plume in the afternoon to dusk sectors [*Darrouzet et al.*, 2009; and references therein]. The oxygen torus is also expected to be eroded and shrunk. If the strong convection causes a rapid drainage of the dayside portion of the oxygen torus, it may be deformed as shown in Figure 9b. It is possible during the storm main phase that the magnetic fiel dipolarization occurs in the ring current region (L∼3.5-5.0) and accelerates locally existing thermal O^+ ions to the ring current energy [*Nosé et al.*, 2010]. Thus, in Figure 9c, thermal O^+ ions in the deformed oxygen torus on the nightside will be accelerated by the magnetic fiel dipolarization. Consequently, the O^+-rich ring current is formed and the oxygen torus is diminishing. After a storm peak, the ring current starts to become axially symmetric and the contracted plasmasphere gradually expands due to the cold plasma replenishment (Figure 9d). The time scale of this replenishment has been estimated to be <28 hrs at L=2.2-3.7 [*Reinisch et al.*, 2004], and 2-3 days at L=2.3-2.6 and >4 days at L>3.3 [*Obana et al.*, 2010]. Therefore, a few or more days later, in late recovery phase, the plasmapause encounters an inner portion of the symmetric ring current (Figure 9e). The heating process of the plasmaspheric electrons, which was discussed in section 6.2, takes place, leading to heat fl w into the underlying ionosphere (Figure 9f, pink arrows). The heat fl w increases the temperature of the ionospheric plasma, and then the scale height of ionospheric ions becomes larger. This causes outfl w of O^+ ions from the ionosphere to the inner magnetosphere (Figure 9f, green arrows). Since the O^+ outfl w occurs in a limited radial distance range, where the expanded plasmasphere meets the inner portion of the ring current, these O^+ ions forms a torus. Then the oxygen torus is created again in the vicinity of the plasmapause (Figure 9a). We attribute the O^+-rich ring current formation to interactions among these 3 elements (i.e., the oxygen torus, the plasmasphere, and the ring current) in this cycle.

Note that the recurrent process discussed above is rather a conjecture based on results from both present and previous studies. Future satellite missions such as the Energization and Radiation in Geospace in Japan and the Radiation Belt Storm Probe in the United States would provide chances to evaluate the conjecture.

7. Summary

This study aims to search for enhancements of O^+ ion density in the deep inner magnetosphere, that is, the oxygen torus, by using the magnetic fiel data and the plasma wave data obtained by the CRRES satellite. We fin 4 events on the dayside and flank sides in which toroidal standing Alfvén waves appeared clearly. From the frequency of the fundamental mode waves, we estimate the magnetospheric local mass density (ρ_L) by solving the MHD wave equation in the Tsyganenko 1989c magnetic fiel model and the mass density distribution model. We also estimate the local electron number density (n_{eL}) from the plasma wave spectrograms by identifying narrow-band emission at the upper-hybrid resonance frequency. Assuming the quasi-neutral condition of plasma, we infer the local average ion mass (M_L) by ρ_L/n_{eL}.

From the profil of n_{eL}, we identify the plasmapause at L=4.6-5.0 (event 1), L=3.5-4.3 (event 2), L=3.4-3.6 (event 3), and L=5.4-6.1 (event 4). M_L is found to be approximately 3 amu well outside these plasmapause (i.e., in the plasma trough). However, M_L shows an enhancement of 7-18 amu in the vicinity of the plasmapause, that is, L∼5.0-5.2 (event 1), L∼4.5-4.8 (event 2), $L\leq$5.6 (event 3), and L∼5.0-6.5 (event 4). These enhancements of M_L in a limited L range indicate the existence of the oxygen torus. Inspection of the Dst index for these 4 events reveals that the oxygen torus is likely to be observed during the late recovery phase or at the end of magnetic storms. The features of the oxygen torus found in this study are quite consistent with those reported by previous studies employing DE-1/RIMS, regarding its radial and MLT distribution, ion composition, and dependence on geomagnetic condition.

Finally, we discuss the oxygen torus in the context of a possible source of the O^+-rich ring current. The oxygen torus exists in the deep inner magnetosphere (L∼3.0-5.0) during the late recovery phase or quiet time. When magnetic storms are initiated, magnetic fiel dipolarization can occur even in deep inner magnetosphere, resulting in local and nonadiabatic acceleration of thermal O^+ ions in the oxygen torus [*Nosé et al.*, 2010]. The accelerated O^+ ions contribute to the ring current and create the O^+-rich ring current. During the storm recovery phase, the plasmasphere expands and encounters the inner portion of the ring current. Coexistence of energetic ring current ions and cold plasmaspheric plasma leads to the Coulomb collision or excitation of the ion cyclotron wave followed by the Landau resonance interaction. In either case, energy transfer from the ring current ions to thermal plasmaspheric electrons takes place. The heated electrons cause increases of the temperature and the scale height of the underlying ionosphere. Thus a large number of O^+ ions fl w out from the ionosphere and form the oxygen torus in a limited L-shell where the ring current and the plasmasphere coexisted. The above process returns to the starting point, that is, the oxygen torus during the late recovery phase or quiet time. Therefore we think that the O^+-rich ring current formation is a recurrent process, in which the oxygen torus, the plasmasphere, and the ring current interact with each other (see Figure 9).

Acknowledgements

The Dst index was provided by the World Data Center for Geomagnetism, Kyoto. The Kp index was provided by H. J. Linthe at the Helmholtz Centre Potsdam, GFZ German Research Centre for Geosciences. The solar wind data were provided from the NASA/GSFC OMNIWeb WWW site. Geomagnetic fiel by the Tsyganenko 1989c model was calculated with GEOPACK routines developed by N. A. Tsyganenko and coded by H. Korth. We are thankful to H. Nakata and Y. Obana for their helpful comments. This work was supported by the Ministry of Education, Science, Sports and Culture, Grant-in-Aid for Young Scientists (B) (grant 22740322). Work at The Johns Hopkins University Applied Physics Laboratory (KT) was supported by NSF grants ATM-0632740 and ATM-0855924.

References

Anderson, B. J., M. J. Engebretson, S. P. Rounds, L. J. Zanetti, and T. A. Potemra (1990), A statistical study of Pc 3-5 pulsations observed by the AMPTE/CCE magnetic field experiment 1. Occurrence distributions, *J. Geophys. Res.*, *95*, 10,495–10,523, doi:10.1029/JA095iA07p10495.

Anderson, R. R., D. A. Gurnett, and D. L. Odem (1992), CRRES plasma wave experiment, *J. Spacecr. Rockets*, *29*, 570–573, doi:10.2514/3.25501.

Carpenter, D. L., and R. R. Anderson (1992), An ISEE/Whistler model of equatorial electron density in the magnetosphere, *J. Geophys. Res.*, *97*, 1097–1108, doi:10.1029/91JA01548.

Chappell, C. R. (1982), Initial observations of thermal plasma composition and energetics from Dynamics Explorer-1, *Geophys. Res. Lett.*, *9*, 929–932, doi:10.1029/GL009i009p00929.

Chappell, C. R., K. K. Harris, and G. W. Sharp (1970), A study of the influenc of magnetic activity on the location of the plasmapause as measured by OGO 5., *J. Geophys. Res.*, *75*, 50–56, doi:10.1029/JA075i001p00050.

Chi, P. J., C. T. Russell, J. C. Foster, M. B. Moldwin, M. J. Engebretson, and I. R. Mann (2005), Density enhancement in plasmasphere-ionosphere plasma during the 2003 Halloween Superstorm: Observations along the 330th magnetic meridian in North America, *Geophys. Res. Lett.*, *32*, L03S07, doi:10.1029/2004GL021722.

Cole, K. D. (1965), Stable auroral red arcs, sinks for energy of Dst main phase, *J. Geophys. Res.*, *70*, 1689–1706, doi:10.1029/JZ070i007p01689.

Comfort, R. H. (1996), Thermal structure of the plasmasphere, *Adv. Space Res.*, *17*(10), 175–184, doi:10.1016/0273-1177(95)00710-V.

Comfort, R. H., I. T. Newberry, and C. R. Chappell (1988), Preliminary statistical survey of plasmaspheric ion properties from observations by DE 1/RIMS, in *Modeling Magnetospheric Plasma*, *Geophys. Monogr. Ser.*, vol. 44, edited by T. E. Moore, and J. H. Waite, Jr., pp. 107–114, AGU, Washington, D.C.

Cornwall, J. M., F. V. Coroniti, and R. M. Thorne (1971), Unifie theory of SAR arc formation at the plasmapause., *J. Geophys. Res.*, *76*, 4428–4445, doi:10.1029/JA076i019p04428.

C:son Brandt, P., S. Ohtani, D. G. Mitchell, M. Fok, E. C. Roelof, and R. Demajistre (2002), Global ENA observations of the storm mainphase ring current: Implications for skewed electric field in the inner magnetosphere, *Geophys. Res. Lett.*, *29*(20), 1954, doi:10.1029/2002GL015160.

Daglis, I. A. (1997), The role of magnetosphere-ionosphere coupling in magnetic storm dynamics, in *Magnetic Storms*, *Geophys. Monogr. Ser.*, vol. 98, edited by B. T. Tsurutani, W. D. Gonzalez, Y. Kamide, and J. K. Arballo, pp. 107–116, AGU, Washington, D.C.

Daglis, I. A. (2006), Ring Current Dynamics, *Space Sci. Rev.*, *124*, 183–202, doi:10.1007/s11214-006-9104-z.

Daglis, I. A., and J. U. Kozyra (2002), Outstanding issues of ring current dynamics, *J. Atmos. Sol. Terr. Phys.*, *64*, 253–264, doi:10.1016/S1364-6826(01)00087-6.

Daglis, I. A., M. Banaszkiewicz, and E. B. Wodnicka (1994), Coupling of the high-latitude and the equatorial magnetosphere during substorms through the transport/acceleration of ionospheric ions, *Proceedings Int. Conf. Substorms-2*, pp. 615–619.

Daglis, I. A., Y. Kamide, C. Mouikis, G. D. Reeves, E. T. Sarris, K. Shiokawa, and B. Wilken (2000), "Fine structure" of the storm-substorm relationship: Ion injections during Dst decrease, *Adv. Space Res.*, *25*, 2369–2372, doi:10.1016/S0273-1177(99)00525-6.

Darrouzet, F., et al. (2009), Plasmaspheric Density Structures and Dynamics: Properties Observed by the CLUSTER and IMAGE Missions, *Space Sci. Rev.*, *145*, 55–106, doi:10.1007/s11214-008-9438-9.

Delcourt, D. C., A. Pedersen, and J. A. Sauvaud (1990), Dynamics of single-particle orbits during substorm expansion phase, *J. Geophys. Res.*, *95*, 20,853–20,865, doi:10.1029/JA095iA12p20853.

Denton, R. E., J. Goldstein, J. D. Menietti, and S. L. Young (2002), Magnetospheric electron density model inferred from Polar plasma wave data, *J. Geophys. Res.*, *107*, 1386, doi:10.1029/2001JA009136.

Denton, R. E., K. Takahashi, R. R. Anderson, and M. P. Wuest (2004), Magnetospheric toroidal Alfvén wave harmonics and the fiel line distribution of mass density, *J. Geophys. Res.*, *109*(A18), A06202, doi:10.1029/2003JA010201.

Feldstein, Y. I., L. A. Dremukhina, U. Mall, and J. Woch (2000), On the two-phase decay of the Dst-variation, *Geophys. Res. Lett.*, *27*, 2813–2816, doi:10.1029/2000GL003783.

Fraser, B. J., J. L. Horwitz, J. A. Slavin, Z. C. Dent, and I. R. Mann (2005), Heavy ion mass loading of the geomagnetic fiel near the plasmapause and ULF wave implications, *Geophys. Res. Lett.*, *32*, L04102, doi:10.1029/2004GL021315.

Gallagher, D. L., P. D. Craven, and R. H. Comfort (2000), Global core plasma model, *J. Geophys. Res.*, *105*, 18,819–18,834, doi:10.1029/1999JA000241.

Gazey, N. G. J., et al. (1996), EISCAT/CRRES observations: nightside ionospheric ion outfl w and oxygen-rich substorm injections, *Ann. Geophys.*, *14*, 1032–1043, doi:10.1007/s005850050364.

Gloeckler, G., F. M. Ipavich, B. Wilken, W. Stuedemann, and D. Hovestadt (1985), First composition measurement of the bulk of the storm-time ring current (1 to 300 keV/e) with AMPTE-CCE, *Geophys. Res. Lett.*, *12*, 325–328, doi:10.1029/GL012i005p00325.

Greenspan, M. E., and D. C. Hamilton (2002), Relative contributions of H^+ and O^+ to the ring current energy near magnetic storm maximum, *J. Geophys. Res.*, *107*, 1043, doi:10.1029/2001JA000155.

Grew, R. S., F. W. Menk, M. A. Clilverd, and B. R. Sandel (2007), Mass and electron densities in the inner magnetosphere during a prolonged disturbed interval, *Geophys. Res. Lett.*, *34*, L02108, doi:10.1029/2006GL028254.

Hamilton, D. C., G. Gloeckler, F. M. Ipavich, B. Wilken, and W. Stuedemann (1988), Ring current development during the great geomagnetic storm of February 1986, *J. Geophys. Res.*, *93*, 14,343–14,355, doi:10.1029/JA093iA12p14343.

Hoffman, R. A. (1988), The magnetosphere, ionosphere, and atmosphere as a system: Dynamics Explorer f ve years later, *Rev. Geophys.*, *26*, 209–214, doi:10.1029/RG026i002p00209.

Horwitz, J. L., R. H. Comfort, and C. R. Chappell (1984), Thermal ion composition measurements of the formation of the new outer plasmasphere and double plasmapause during storm recovery phase, *Geophys. Res. Lett.*, *11*, 701–704, doi:10.1029/GL011i008p00701.

Horwitz, J. L., R. H. Comfort, L. H. Brace, and C. R. Chappell (1986), Dual-spacecraft measurements of plasmasphere-ionosphere coupling, *J. Geophys. Res.*, *91*, 11,203–11,216, doi:10.1029/JA091iA10p11203.

Horwitz, J. L., R. H. Comfort, P. G. Richards, M. O. Chandler, C. R. Chappell, P. Anderson, W. B. Hanson, and L. H. Brace (1990), Plasmasphere-ionosphere coupling 2: Ion composition measurements at plasmaspheric and ionospheric altitudes and comparison with modeling results, *J. Geophys. Res.*, *95*, 7949–7959, doi:10.1029/JA095iA06p07949.

Johnson, M. H., and J. Kierein (1992), Combined release and radiation effects satellite (CRRES): Spacecraft and mission, *J. Spacecr. Rockets*, *29*, 556–563, doi:10.2514/3.55641.

Kamide, Y., et al. (1997), Magnetic storms: Current understanding and outstanding questions, in *Magnetic Storms*, *Geophys. Monogr. Ser.*, vol. 98, edited by B. T. Tsurutani, W. D. Gonzalez, Y. Kamide, and J. K. Arballo, pp. 1–19, AGU, Washington, D.C.

Krimigis, S. M., R. W. McEntire, T. A. Potemra, G. Gloeckler, F. L. Scarf, and E. G. Shelley (1985), Magnetic storm of September 4, 1984 - A synthesis of ring current spectra and energy densities measured with AMPTE/CCE, *Geophys. Res. Lett.*, *12*, 329–332, doi:10.1029/GL012i005p00329.

Le, G., C. Russell, and K. Takahashi (2004), Morphology of the ring current derived from magnetic fiel observations, *Ann. Geophys.*, *22*, 1267–1295, doi:10.5194/angeo-22-1267-2004.

LeDocq, M. J., D. A. Gurnett, and R. R. Anderson (1994), Electron number density fluctuation near the plasmapause observed by the CRRES spacecraft, *J. Geophys. Res.*, *99*, 23,661–23,671, doi:10.1029/94JA02294.

Lui, A. T. Y. (1993), Radial transport of storm time ring current ions, *J. Geophys. Res.*, *98*, 209–214, doi:10.1029/92JA02079.

Lui, A. T. Y., R. W. McEntire, S. M. Krimigis, and E. P. Keath (1986), Acceleration of energetic oxygen ($E>137$ keV) in the storm-time ring current, in *Ion Acceleration in the Magnetosphere and Ionosphere*, *Geophys. Monogr. Ser.*, vol. 38, edited by T. Chang, pp. 149–152, AGU, Washington, D.C.

Lui, A. T. Y., R. W. McEntire, and S. M. Krimigis (1987), Evolution of the ring current during two geomagnetic storms, *J. Geophys. Res.*, *92*, 7459–7470, doi:10.1029/JA092iA07p07459.

Maeda, N., S. Takasaki, H. Kawano, S. Ohtani, P. Decreau, J. Trotignon, S. Solovyev, D. Baishev, and K. Yumoto (2009), Simultaneous observations of the plasma density on the same fiel line by the CPMN ground magnetometers and the Cluster satellites, *Adv. Space Res.*, *43*, 265–272, doi:10.1016/j.asr.2008.04.016.

McEntire, R. W., A. T. Y. Lui, S. M. Krimigis, and E. P. Keath (1985), AMPTE/CCE energetic particle composition measurements during the September 4, 1984 magnetic storm, *Geophys. Res. Lett.*, *12*, 317–320, doi:10.1029/GL012i005p00317.

Mitchell, D. G., K. C. Hsieh, C. C. Curtis, D. C. Hamilton, H. D. Voss, E. C. Roelof, and P. C:son-Brandt (2001), Imaging two geomagnetic storms in energetic neutral atoms, *Geophys. Res. Lett.*, *28*, 1151–1154, doi:10.1029/2000GL012395.

Mitchell, D. G., P. C:son Brandt, E. C. Roelof, D. C. Hamilton, K. C. Retterer, and S. Mende (2003), Global imaging of O^+ from IMAGE/HENA, *Space Sci. Rev.*, *109*, 63–75, doi:10.1023/B:SPAC.0000007513.55076.00.

Moldwin, M. B., L. Downward, H. K. Rassoul, R. Amin, and R. R. Anderson (2002), A new model of the location of the plasmapause: CRRES results, *J. Geophys. Res.*, *107*, 1339, doi:10.1029/2001JA009211.

Nakabe, S., T. Iyemori, M. Sugiura, and J. A. Slavin (1997), A statistical study of the magnetic fiel structure in the inner magnetosphere, *J. Geophys. Res.*, *102*, 17,571–17,582, doi:10.1029/97JA01181.

Newberry, I. T., R. H. Comfort, P. G. Richards, and C. R. Chappell (1989), Thermal He^+ in the plasmasphere: Comparison of observations with numerical calculations, *J. Geophys. Res.*, *94*, 15,265–15,276, doi:10.1029/JA094iA11p15265.

Nosé, M., S. Taguchi, K. Hosokawa, S. P. Christon, R. W. McEntire, T. E. Moore, and M. R. Collier (2005), Overwhelming O^+ contribution to the plasma sheet energy density during the October 2003 superstorm: Geotail/EPIC and IMAGE/LENA observations, *J. Geophys. Res.*, *110*, A09S24, doi:10.1029/2004JA010930.

Nosé, M., A. Ieda, and S. P. Christon (2009), Geotail observations of plasma sheet ion composition over 16 years: On variations of average plasma ion mass and O^+ triggering substorm model, *J. Geophys. Res.*, *114*, A07223, doi:10.1029/2009JA014203.

Nosé, M., H. Koshiishi, H. Matsumoto, P. C:son Brandt, K. Keika, K. Koga, T. Goka, and T. Obara (2010), Magnetic fiel dipolarization in the deep inner magnetosphere and its role in development of O^+-rich ring current, *J. Geophys. Res.*, *115*, A00J03, doi:10.1029/2010JA015321.

Obana, Y., F. W. Menk, and I. Yoshikawa (2010), Plasma refillin rates for L=2.3-3.8 flu tubes, *J. Geophys. Res.*, *115*(A14), A03204, doi:10.1029/2009JA014191.

Ohtani, S., P. C. Brandt, D. G. Mitchell, H. Singer, M. Nosé, G. D. Reeves, and S. B. Mende (2005), Storm-substorm relationship: Variations of the hydrogen and oxygen energetic neutral atom intensities during storm-time substorms, *J. Geophys. Res.*, *110*, A07219, doi:10.1029/2004JA010954.

Reinisch, B. W., X. Huang, P. Song, J. L. Green, S. F. Fung, V. M. Vasyliunas, D. L. Gallagher, and B. R. Sandel (2004), Plasmaspheric mass loss and refillin as a result of a magnetic storm, *J. Geophys. Res.*, *109*(A18), A01202, doi:10.1029/2003JA009948.

Roberts, W. T., Jr., J. L. Horwitz, R. H. Comfort, C. R. Chappell, J. H. Waite, Jr., and J. L. Green (1987), Heavy ion density enhancements in the outer plasmasphere, *J. Geophys. Res.*, *92*, 13,499–13,512, doi:10.1029/JA092iA12p13499.

Roeder, J. L., J. F. Fennell, M. W. Chen, M. Schulz, M. Grande, and S. Livi (1996), CRRES observations of the composition of the ring-current ion populations, *Adv. Space Res.*, *17*, 17–24, doi:10.1016/0273-1177(95)00689-C.

Sánchez, E. R., B. H. Mauk, and C. Meng (1993), Adiabatic vs. non-adiabatic particle distributions during convection surges, *Geophys. Res. Lett.*, *20*, 177–180, doi:10.1029/93GL00237.

Singer, H. J., D. J. Southwood, R. J. Walker, and M. G. Kivelson (1981), Alfvén wave resonances in a realistic magnetospheric magnetic fiel geometry, *J. Geophys. Res.*, *86*, 4589–4596, doi:10.1029/JA086iA06p04589.

Singer, H. J., W. P. Sullivan, P. Anderson, F. Mozer, P. Harvey, J. Wygant, and W. McNeil (1992), Fluxgate magnetometer instrument on the CRRES, *J. Spacecr. Rockets*, *29*, 599–601, doi:10.2514/3.25506.

Takahashi, K., and B. J. Anderson (1992), Distribution of ULF energy ($f <$ 80 mHz) in the inner magnetosphere: A statistical analysis of AMPTE CCE magnetic fiel data, *J. Geophys. Res.*, *97*, 10,751–10,773, doi:10.1029/92JA00328.

Takahashi, K., and R. E. Denton (2007), Magnetospheric seismology using multiharmonic toroidal waves observed at geosynchronous orbit, *J. Geophys. Res.*, *112*(A11), A05204, doi:10.1029/2006JA011709.

Takahashi, K., R. E. Denton, R. R. Anderson, and W. J. Hughes (2004), Frequencies of standing Alfvén wave harmonics and their implication for plasma mass distribution along geomagnetic fiel lines: Statistical analysis of CRRES data, *J. Geophys. Res.*, *109*, A08202, doi:10.1029/2003JA010345.

Takahashi, K., R. E. Denton, R. R. Anderson, and W. J. Hughes (2006), Mass density inferred from toroidal wave frequencies and its comparison to electron density, *J. Geophys. Res.*, *111*, A01201, doi:10.1029/2005JA011286.

Takahashi, K., S. Ohtani, R. E. Denton, W. J. Hughes, and R. R. Anderson (2008), Ion composition in the plasma trough and plasma plume derived from a Combined Release and Radiation Effects Satellite magnetoseismic study, *J. Geophys. Res.*, *113*(A12), A12203, doi:10.1029/2008JA013248.

Taylor, H. A., Jr., H. C. Brinton, and M. W. Pharo, III (1968), Contraction of the Plasmasphere during Geomagnetically Disturbed Periods, *J. Geophys. Res.*, *73*, 961–968, doi:10.1029/JA073i003p00961.

Terada, N., T. Iyemori, M. Nosé, T. Nagai, H. Matsumoto, and T. Goka (1998), Storm-time magnetic fiel variations observed by the ETS-VI satellite, *Earth Planets Space*, *50*, 853–864.

Tsyganenko, N. A. (1989), A magnetospheric magnetic fiel model with a warped tail current sheet, *Planet. Space Sci.*, *37*, 5–20, doi:10.1016/0032-0633(89)90066-4.

Yau, A. W., P. H. Beckwith, W. K. Peterson, and E. G. Shelley (1985), Long-term (solar cycle) and seasonal variations of upfl wing ionospheric ion events at DE 1 altitudes, *J. Geophys. Res.*, *90*, 6395–6407, doi:10.1029/JA090iA07p06395.

R. R. Anderson, Department of Physics and Astronomy, University of Iowa, Iowa City, IA 52242-1479, USA. (roger-r-anderson@uiowa,edu)

M. Nosé, Data Analysis Center for Geomagnetism and Space Magnetism, Graduate School of Science, Kyoto University, Oiwake-cho, Kitashirakawa, Sakyo-ku, Kyoto 606-8502, Japan. (nose@kugi.kyoto-u.ac.jp)

H. J. Singer, NOAA/National Weather Service, National Centers for Environmental Prediction, Space Weather Prediction Center, 325 Broadway, Boulder CO 80305, USA. (howard.singer@noaa.gov)

K. Takahashi, Applied Physics Laboratory, Johns Hopkins University, 11100 Johns Hopkins Road, Laurel, MD 20723-6099, USA. (kazue.takahashi@jhuapl.edu)

Figure 1. Orbits of the CRRES satellite in solar magnetospheric (SM) coordinates for 4 events.

Figure 2. (Top) The magnetic fiel variations in the D component (ΔB_D) for event 1, that is, for 1130-1500 UT on 27 August 1991 and Orbit 961. ΔB_D is created from the observed fiel by subtracting the IGRF model fiel and by low-pass filterin with a cutoff period of 30 s. (Bottom) Dynamic display of the power spectral density of ΔB_D. Open circles represent the fundamental mode frequency of the standing Alfvén waves.

Figure 3. The same as Figure 2 except for event 2, that is, for 1200-1530 UT on 11 September 1991 and Orbit 996.

Figure 4. The same as Figure 2 except for event 3, that is, for 0330-0700 UT on 24 July 1991 and Orbit 881.

Figure 5. The same as Figure 2 except for event 4, that is, for 0930-1300 UT on 29 August 1990 and Orbit 84.

Figure 6. From left to right, results of observations and calculation for events 1-4 are displayed. (Top row) The fundamental mode frequency (f_1) of the standing Alfvén wave, which are identical to the open circles in the bottom panels of Figures 2-5. (2nd row) The magnetospheric local mass density (ρ_L) estimated from f_1. Error bas indicate the range of ρ_L when f_1 ranges from $f_1 + \frac{1}{2}\Delta f$ to $f_1 - \frac{1}{2}\Delta f$. (3rd row) The local electron number density (n_{eL}) derived from the plasma wave spectrograms by identifying the upper hybrid resonance emission. (4th row) The local average plasma mass (M_L) calculated from ρ_L/n_{eL}.

Figure 7. The same as panels in the 3rd and 4th rows of Figure 6, except for being plotted against the L value.

Figure 8. The Dst index for events 1-4. Closed circles in the bottom indicate the time intervals shown in Figures 2-5.

Figure 9. A schematic figur depicting a proposed recurrent process of the O^+-rich ring current formation.

Figure 1

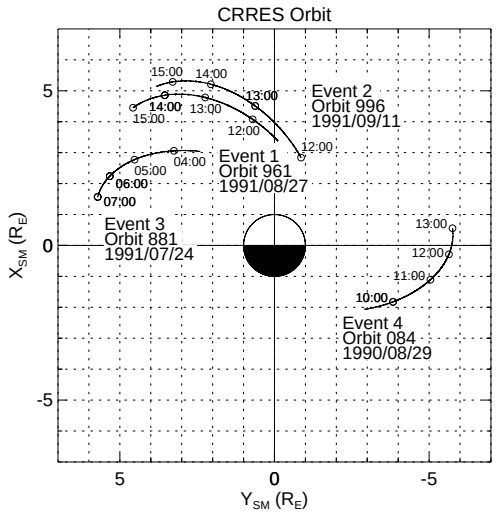

Figure 2

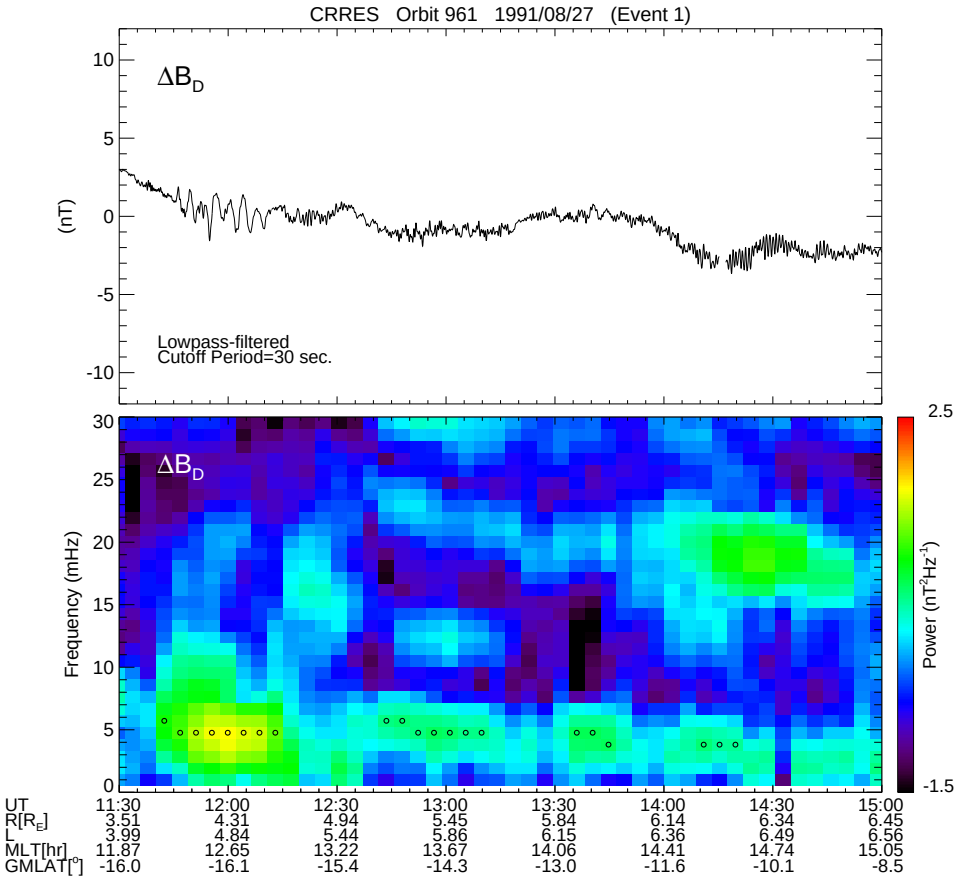

Figure 3

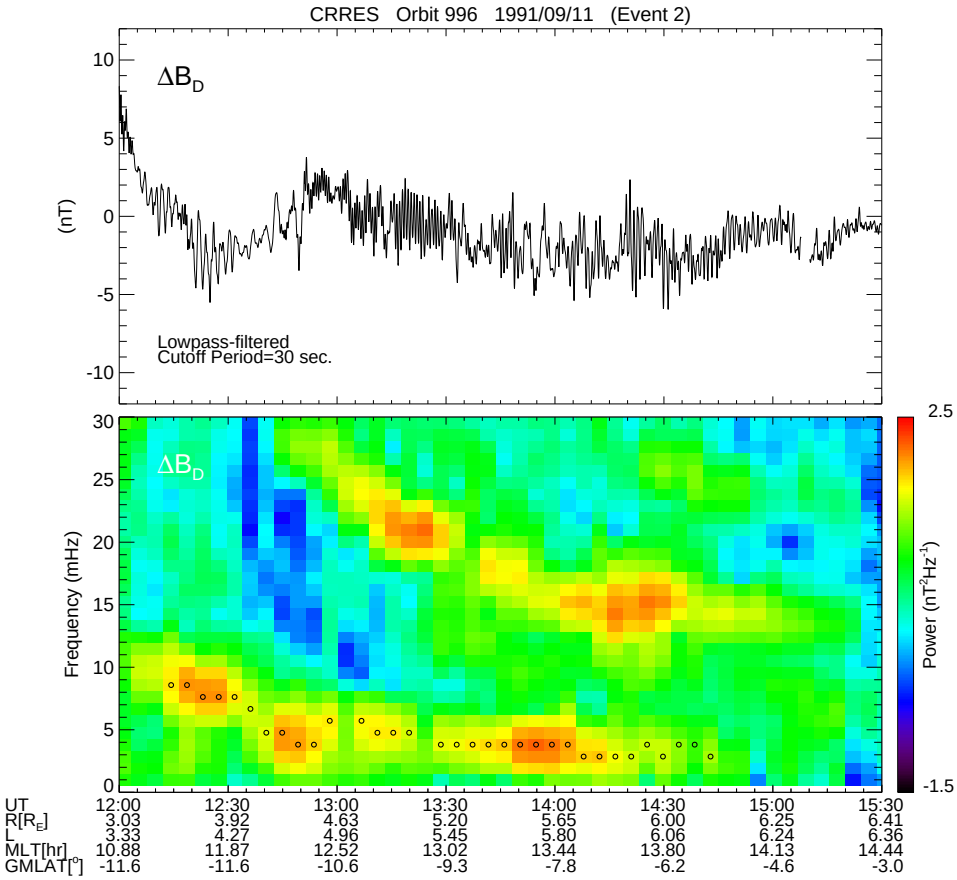

Figure 4

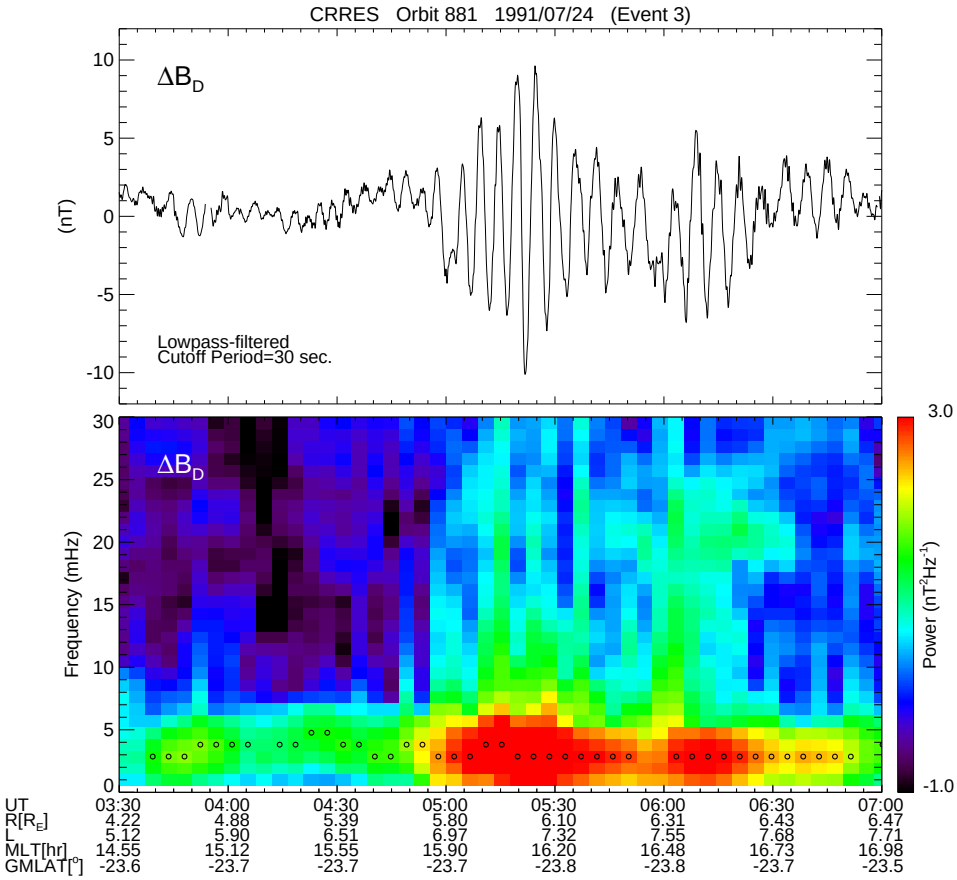

Figure 5

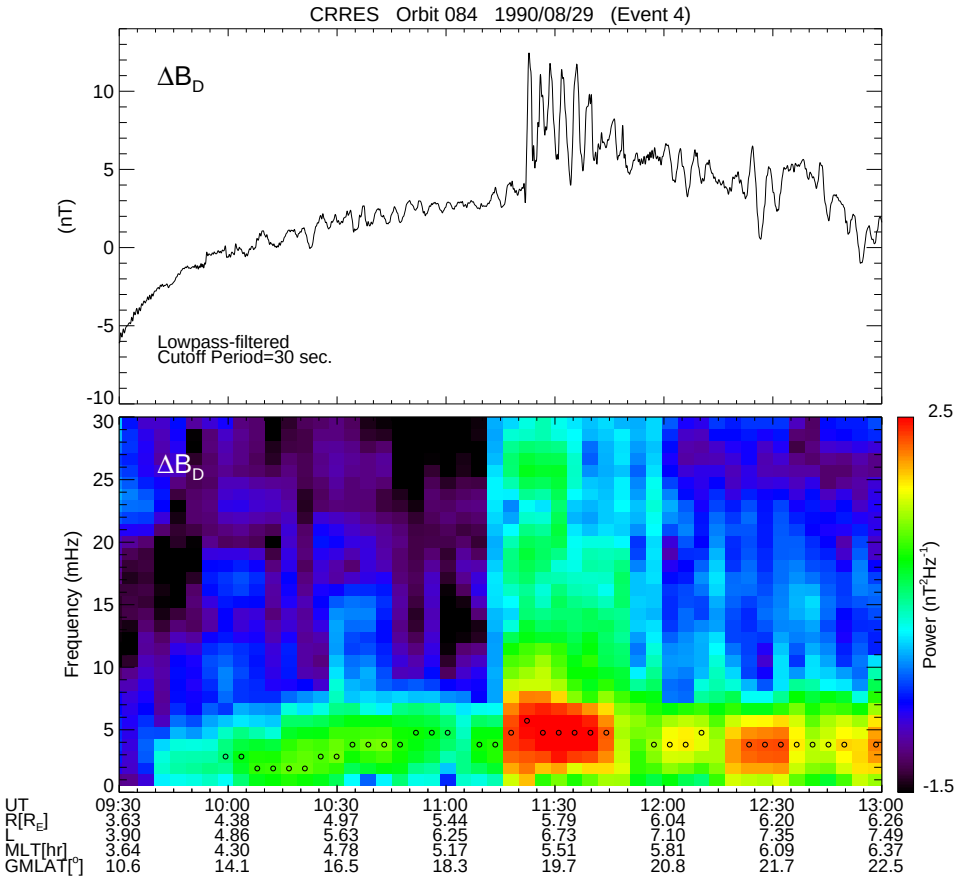

Figure 6

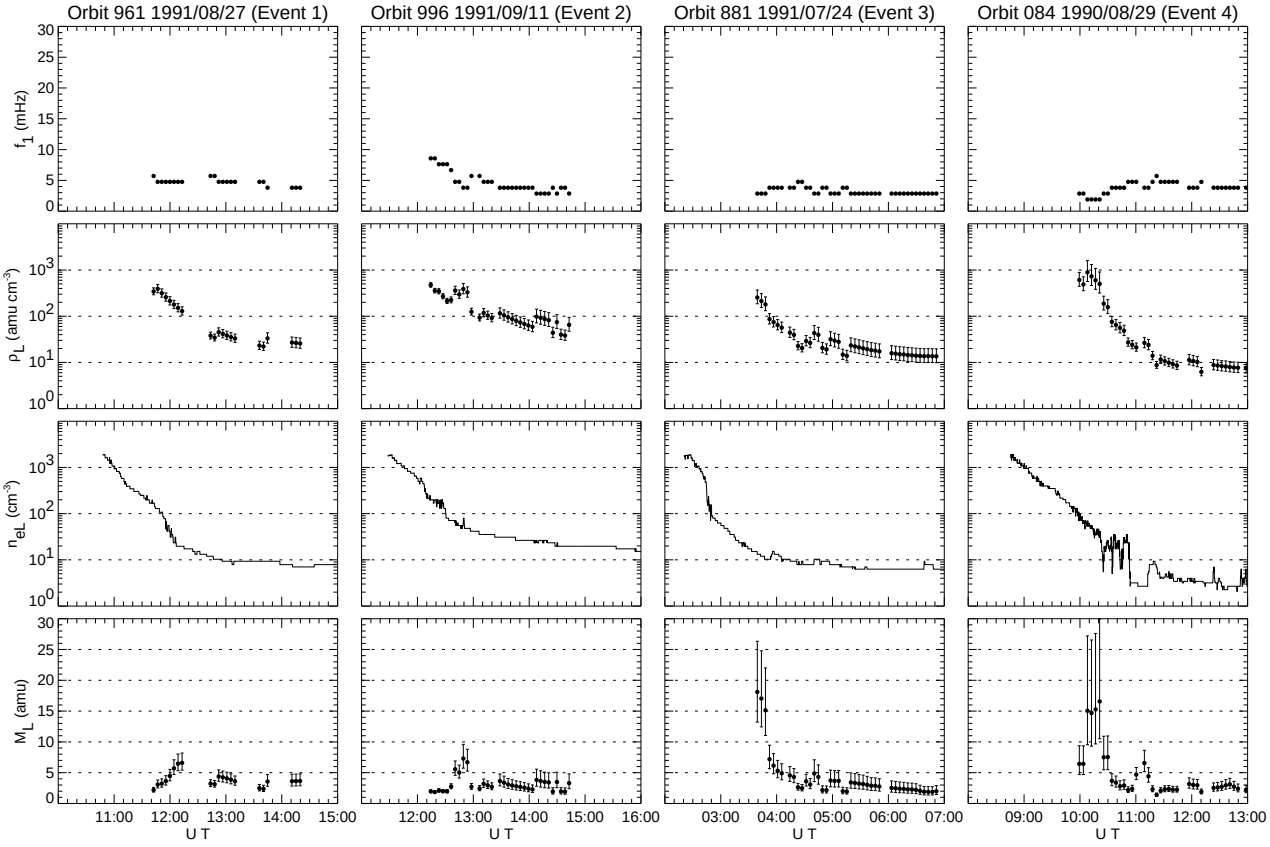

Figure 7

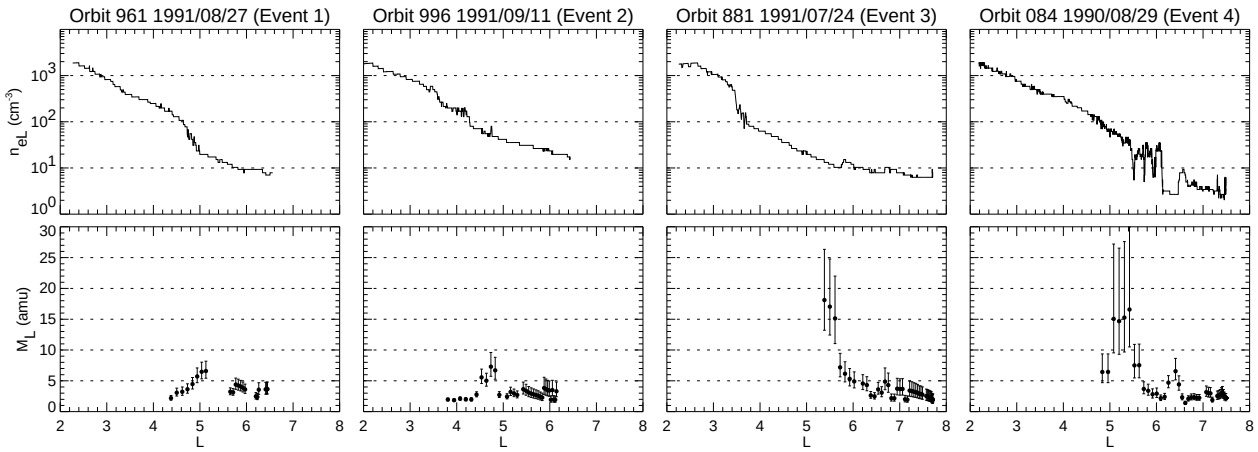

Figure 8

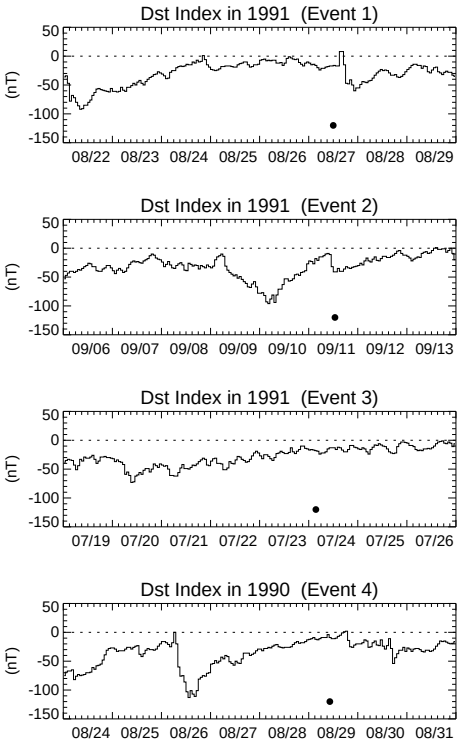

Figure 9